Dome-shaped mmWave Lens Antenna Optimization for Wide-angle Scanning and Scan Loss Mitigation using Geometric Optics and Multiple Scattering

Youngno Youn, Jaehong Choi, Daehyeon Kim, Ahmed Abdelmottaleb Omar, Jaehyun Choi, Suho Chang, Inseop Yoon, Seung-Tae Ko, Jungyub Lee, Youngju Lee, Mobayode O. Akinsolu, *Senior Member, IEEE*, Bo Liu, *Senior Member, IEEE* and Wonbin Hong, *Senior Member, IEEE*

***Abstract*— This paper presents a new accurate and efficient design methodology for complex integrated lens antenna (ILA), to achieve wide-angle beam coverage with scan loss mitigation at the millimeter-wave (mmWave) spectrum. The proposed ILA comprises inhomogeneous curvatures with internal and external center off-sets, in which multiple parameters instigate high order and non-linear behaviors. A two-dimensional (2-D) ray-tracing model is used to estimate the refractions on the elliptically curved boundaries based on geometrical optics. This approach is integrated into the particle swarm optimization of the 2-D ray-tracing model to determine the near-optimum geometric configuration of the ILA. Denoted as Geometric Optics-based Multiple Scattering (GOMS), the computational memory usage is reduced by a factor of 10,000 using this approach. The devised ILA achieves a wide-angle beam coverage of 156° with a scan loss of 2.10 dB alongside a broad impedance bandwidth of 35.0 GHz to 42.0 GHz. The measurement results for the performance of the fabricated prototype of the ILA validate the wide-angle scanning with scan loss mitigation inferred from the simulation results. This confirms the effectiveness of this method for complex design challenges involving multi-variants and restricted computational resources.**

***Index Terms*— Wide-angle scanning, scan loss mitigation, integrated lens antenna, geometric optics, particle swarm optimization.**

I. Introduction

THE fifth-generation (5G) wireless communication new radio exploits millimeter-wave (mmWave) frequency spectrum (10 – 100 GHz) for higher data throughput [1], making free-space path loss one of the major factors that affect the link budget [2]. In addition to free-space path loss, wireless communication in the mmWave spectrum also faces greater diffraction and penetration losses for non-line-of-sight scenarios [3], [4]. To overcome these issues, high gain and beam scanning antennas are imperative for mmWave wireless communication [5].

High gain and directional antennas are often realized using phased array configurations. The design and implementation of these phased array require many radiofrequency (RF) paths, in which phase shifters and power amplifiers account for more than 60% of the total power consumption. Therefore, the reduction of power consumption becomes a critical issue. This can be potentially achieved through the enhancement of hardware efficiency [6]. In this regard, the implementation of wide-beam coverage antennas for reducing the number of sectors could be an effective strategy as carried out in [7]. However, in the case of conventional planar phased arrays, the reduced antenna effective aperture degrades the far-field radiation gain and, scan loss, due to the broadening of the beam width when the main beam peak is steered beyond 60° [8].

An alternate solution is the integrated lens antenna (ILA) that enlarges the antenna effective aperture while maintaining high gain and low sidelobe level [9]-[11]. ILAs are a good choice because they are highly compatible with conventional phased array antennas [12]-[14]. Conventional ILA geometries such as spherical, extended hemispherical and tangent ogive geometries are often analyzed and characterized using optics-based estimations [9]-[11]. However, since these canonical geometries limit the degree of freedom of the design, they often degrade the radiation performance of the ILA, mainly in terms of beam scanning angle, side lobe level and scan loss. A possible way to overcome the inherent limitations of conventional ILA geometries is the adoption of complex ILA geometries with multiple parameters that theoretically allow for high dimensional order and non-linear behavior [12].

Manuscript received XXXX XX, XXXX. This work was supported by Samsung Electronics Co., Ltd. and Next Generation Engineering Research Program of National Research Foundation of Korea (NRF) (No.2019H1D8A2106519) (Corresponding author: *Wonbin Hong*)

Youngno Youn, Jaehong Choi, Daehyeon Kim, Suho Chang and Wonbin Hong are with the Department of Electrical Engineering Pohang University of Science and Technology (POSTECH), Pohang, 37673, Republic of Korea. (e-mail: whong@postech.ac.kr)

Ahmed Abdelmottaleb Omar is with University of Wisconsin-Madison, Electrical and Computer Engineering, Madison, WI, USA.

Jaehyun Choi is with LG Innotek Inc, Gangseo-gu, Seoul 07796, South Korea.

Inseop Yoon, Seung-Tae Ko, Jungyub Lee, and Youngju Lee are with Samsung Electronics, Suwon, 16677, Republic of Korea.

M.O. Akinsolu is with the Faculty of Arts, Science and Technology, Wrexham Glyndwr University, Wrexham LL11 2AW, U.K.

Bo Liu is with James Watt School of Engineering, University of Glasgow, G12 8QQm Scotland.

This paper is an expanded version of a conference paper presented at 2021 IEEE International Symposium on Antennas and Propagation and USNC-URSI Radio Science Meeting, Singapore.

Color versions of one or more of the figures in this article are available online at http://ieeexplore.ieee.org.

Classical design methods such as quasi-optical analysis that employ analytical models can be used to realize complex ILA geometries, However, they are often inaccurate and infeasible for real-world applications since in many cases, the modeling process do not consider the radiation characteristics of the feeding source [15]. To enhance the analysis and characterization of complex ILA geometries, numerical models and full-wave simulations have become a widely accepted convention due to their improved accuracy and reliability. However, for very complex geometries having several design parameters with interdependent topological features and material compositions, the entire design procedure is often computationally expensive. Hence, improving such simulation-driven complex ILA geometries for between performance is not very straightforward as discussed in Section II.C.

In this paper, a new class of ILA design methodology for achieving wide-angle beam coverage and mitigating scan loss at the mmWave spectrum is proposed by integrating the analytical model with the EM model of the ILA [16], [17]. At the preliminary design stage, a sequential geometric optics (GO)-based ray tracing two-dimensional (2-D) calculation is implemented as an analytical model function to determine the near-optimum geometrical parameters for the numerical model of the ILA via evolutionary computation (see Section II. C). The near-optimum parametric information from the preliminary design stage is then used to update the EM model of the ILA to formulate a design that exhibits a good wide-beam coverage and other desirable radiation properties. The devised wide-beam coverage ILA can reduce the number of transceivers and the antenna size to alleviate the hardware installation costs in the case of the base station [7], [18].

This paper is organized as follows. In Section II, the geometric optics-based multiple scattering (GOMS) approach is detailed in four steps. In Section III the optimized ILA is validated by measurements. The conclusions are drawn in Section IV.

II.GOMS-BASED ILA DESIGN PROCEDURE

Design optimization plays a critical role in the present-day designs of antennas, where multiple interconnected critical and sensitive design parameters are required to be optimized to meet multiple (stringent) design specifications [19]-[20]. As a workaround, conventional approaches such as experience-driven trial and error and parameter sweeping, or parametric study are often exhaustive without any guarantee of successful outcomes [21]. Hence, the need for the design automation of antennas via modern optimization algorithms.

Antenna design optimization methods are broadly grouped into local and global optimization methods [21]-[23]. Since local optimization methods require a very accurate design to obtain reasonably accurate results, these methods are not predominantly used in the design of real-life antennas due to the lack of the initial design information [24]-[25]. On the other hand, global optimization methods do not require initial designs and their

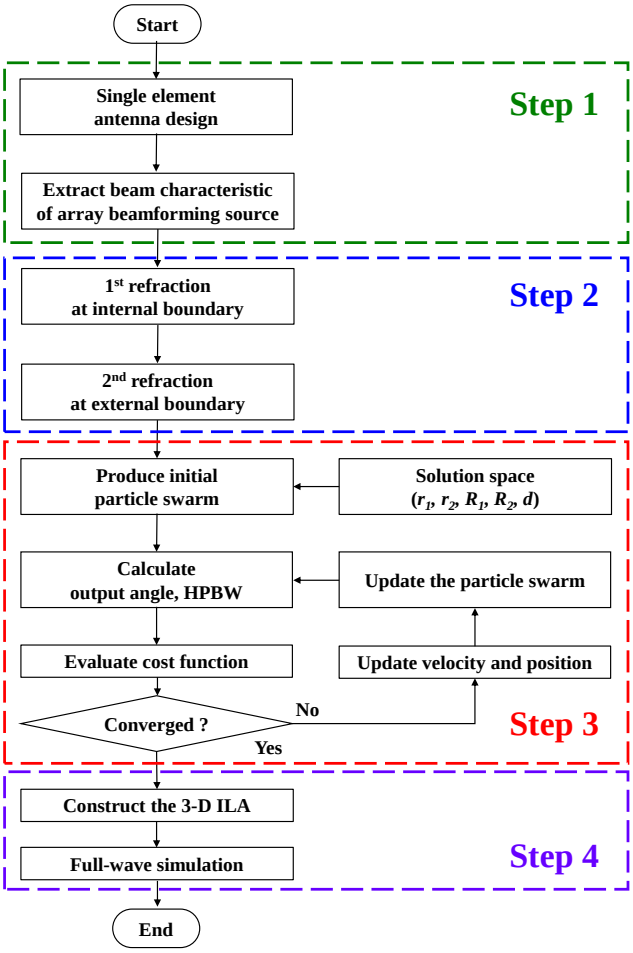

Fig. 1. Flow chart of the proposed Geometric Optics-based Multiple Scattering (GOMS) approach.

explorative ability makes them overcome the drawback of getting trapped in local optima that local optimization methods suffer from. As a result, global optimization methods, particularly, evolutionary algorithms (EAs, a subset of evolutionary computation) are widely used for antenna optimization [26]-[29].

Despite their strong optimization ability, EAs suffer from the drawback of requiring a large amount of full-wave EM simulations to obtain good results for the simulation-driven global optimization of antennas [21], [27], [29]-[30]. To circumvent this issue, machine learning (ML) is incorporated into the optimization kernels of EAs to predict the performances of candidate antenna designs in the optimization process [20], [31]-[32]. In this way, the efficiency of EAs is improved by replacing a good amount of full-wave EM simulations with ML-based predictions in the optimization process. This kind of method shows many successes when each EM simulation costs a reasonable time (e.g. 5-30 minutes). For example, in [33], the expected 3-month running was reduced to 3 days, obtaining a high-performance design. However, when each EM simulation costs a long time (e.g. more than a few hours), they are also unaffordable because at least a few hundred EM simulations are needed.

In this work, a single full-wave EM simulation of the EM model discretized using 228,482 mesh cells in Ansys Electronic

Desktop (EDT) and analyzed using the High-Frequency Structure Simulator (HFSS) costs about a whole day. Hence, even an ML-assisted global optimization-based antenna design approach is not affordable for this case. Therefore, an analytical model is built to approximate the EM model. The calculation of this analytical model costs a few seconds, addressing the challenge of time consumption when using EAs. Through the optimization of the analytical model, a near-optimum solution can be obtained, which will be used for the EM model for verification. The flow chart of the design process is shown in Fig. 1 and four steps are involved in devising the proposed antenna.

As illustrated in Fig. 1, the first step is to design, the EM model of an 8×16 phased array feeding source and extract radiation characteristics such as gain and half-power beamwidth (HPBW) using full-wave EM simulation. The second step is to establish a reasonably accurate 2-D ray tracing model via GO estimation to have reduced computational time. The third step is to undertake a global optimization of the 2-D ray tracing model to determine the near-optimum parametric information for the EM model of the proposed ILA. A standard EA, particle swarm optimization (PSO), is used for the optimization of the 2-D ray tracing model. As said above, PSO does not require an initial design and it prevents the optimization procedure from getting trapped in local optima to a large extent, even under high-order and non-linear constraints [19], [20]. In the fourth step, the optimized ILA is simulated by using MC Nylon (ε_r = 3.20, tan (δ) = 0.02) material for verifying its wide-angle scanning abilities. The MC Nylon was the only material available at the time of this study.

A. Feeding Array Source Design

A microstrip patch antenna is implemented as the feeding source for the ILA due to its lightweight, low profile, and low cost, which are essential features for base stations and access points [33]. To achieve a broadband operational bandwidth, a parasitic patch element is stacked on the main radiator patch element, as shown in Fig. 2 (a). To enhance the isolation between adjacent elements, shielding cases and via wall structures are employed for mutual coupling and undesired surface current suppression. The stacked circular patch antenna is analyzed using Ansys EDT-HFSS. The operating center frequency is 39.0 GHz and the operating impedance bandwidth is from 35.0 GHz to 42.5 GHz, as shown in Fig. 2 (b). This devised single element is developed into an 8×16 phased array antenna by using periodic boundaries for the beamforming simulation. The active reflection coefficients are simulated for calculating the coupling coefficients between adjacent elements. Considering the symmetricity of the phased array, reflection coefficients of 4 ports (port #1, port #4, port #57, and port #60) are evaluated and the calculated results demonstrate the impedance bandwidth of the phased array is maintained for the single element. In Fig. 2 (c), the simulated radiation patterns are normalized according to the maximum gain of 25.6 dBi at 0˚. These simulated results exhibit a scan loss of 2.70 dB when the main beam peak is located at 45˚ in the azimuth plane

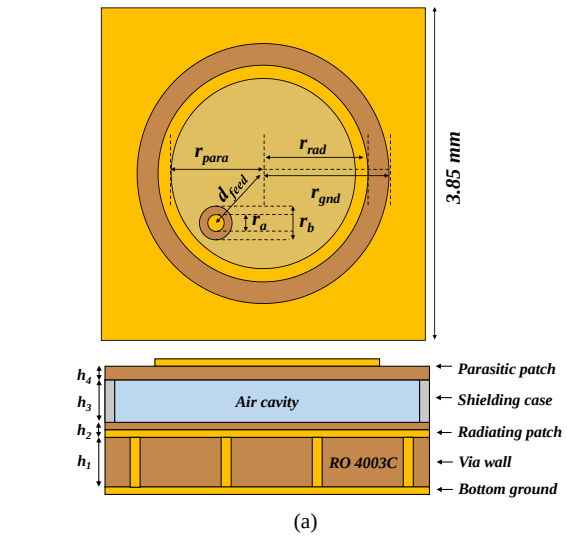

(a)

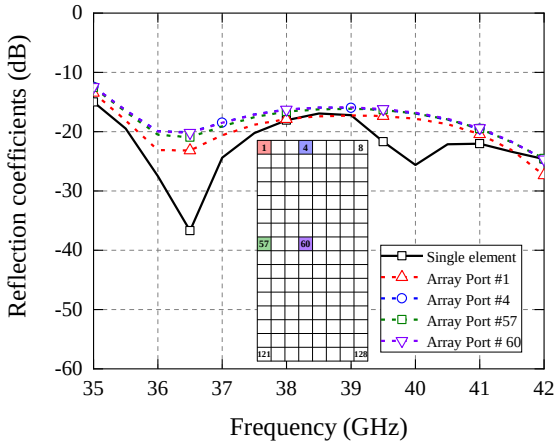

(b)

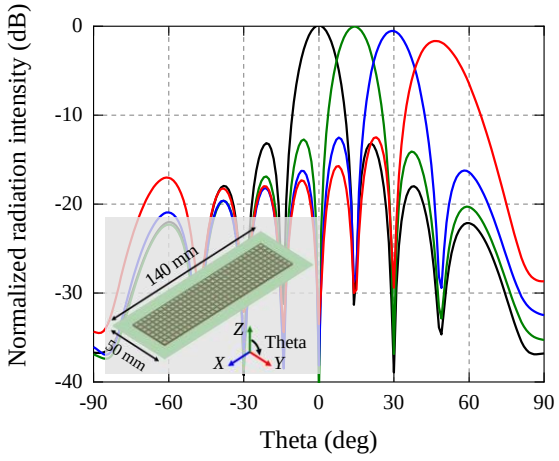

(c)

Fig. 2. (a) Top and side view of the circular stacked patch antenna (b) simulated active reflection coefficients (c) simulated results of phased array antenna at 39.0 GHz in *yz*-plane. The dimensions of the antenna are r_a = 0.20 mm, r_b = 0.40 mm, r_{para} = 1.10 mm, r_{rad} = 1.25mm, r_{gnd} = 1.50 mm, d_{feed} = 1.10 mm, h_1 = 0.435 mm, h_2 = 0.125 mm, h_3 = 0.425 mm, h_4 = 0.107 mm.

(*yz*-plane). In addition, the HPBW for 0˚, 15˚, 30˚, 45˚ incidence in *yz*-plane are 12.5˚, 13.2˚, 14.6˚, 18.0˚, respectively. These

This article has been accepted for publication in IEEE Journal on Multiscale and Multiphysics Computational Techniques. This is the author's version which has not been fully edited and content may change prior to final publication. Citation information: DOI 10.1109/JMMCT.2022.3180550

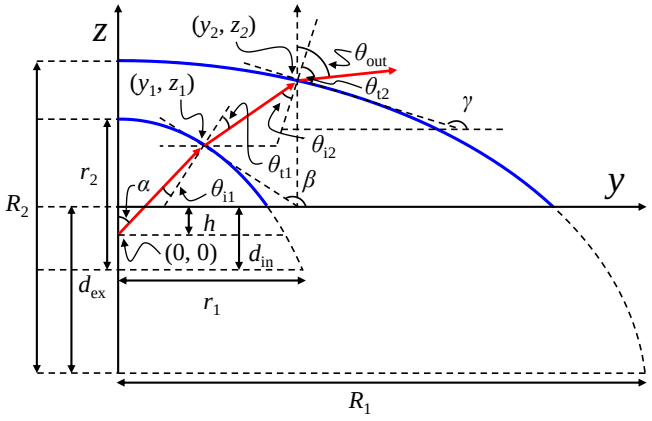

Fig. 3. Geometry of the proposed ILA.

radiation characteristics are used for the 2-D ray-tracing model estimation in the next section.

B. GO-based Ray-tracing Model Estimation for the Dielectric Lens

The radiated wave front from the phased array presented in this work can be assumed to be a ray whose trajectory can be determined approximately using the GO-based estimations [35]. For the dielectric lens, a double-elliptical configuration is adopted for achieving wide-angle scanning capabilities and the off-centered elliptical curvatures enhance the output scanning angle to have a dome-shaped lens as shown in Fig. 3. In the first refraction of the oblique incident wave for the internal elliptically-curved boundary (r_1, r_2) with off-center (d_{in}) and the separation (h) along the r_2 axis is calculated as follows

$$n_1 \sin\theta_{i1} = n_1 \sin(\alpha + \beta - \pi) = n_2 \sin\theta_{t1} \quad (1)$$

$$\beta = \tan^{-1}\left(-\frac{y_1}{z_1 + d_{in} - h}\frac{{r_2}^2}{{r_1}^2}\right) \quad (2)$$

where α is the beam scanning angle of the feeding source, tan (β) is the slope of the tangent line to the internal elliptically curved boundary (r_1, r_2), and n_1, n_2 are the refractive indices of materials. Considering the integration with the phased array antenna, the separation between the feeding source and the ILA (h) is set to be 10 mm. To have wide-angle scanning, the proposed dome- shaped dielectric lens adopts inhomogeneous eccentricity of the internal elliptically curved boundary (r_1, r_2) and external elliptically curved boundary (R_1, R_2) with internal off-set (d_{in}) and external off-set (d_{ex}). The refracted wave on the internal elliptically curved boundary (r_1, r_2) propagates into the dielectric lens and the second refracted angle θ_{t2}, output angle θ_{out} is deduced as follows:

$$\theta_{t2} = \sin^{-1}((n_2/n_1) * \sin(\gamma - \beta + \theta_{t1})) \quad (3)$$

$$\gamma = \tan^{-1}\left(-\frac{y_2}{z_2 + d_{ex}}\frac{{R_2}^2}{{R_1}^2}\right) \quad (4)$$

$$\theta_{out} = \alpha - \theta_{i1} + \theta_{t1} - \theta_{i2} + \theta_{t2} \quad (5)$$

where tan (γ) is the curvature of the external elliptically curved boundary (R_1, R_2). Using the equations derived above, an analytical function for the ray-tracing 2-D model is formulated to estimate the main beam peak angle and the half-power beamwidth according to eq. (5) for any given geometry of the ILA. These estimates are employed for evaluating the fitness of the PSO-driven global optimization of the geometry of the dome-shaped dielectric lens as discussed in the next subsection.

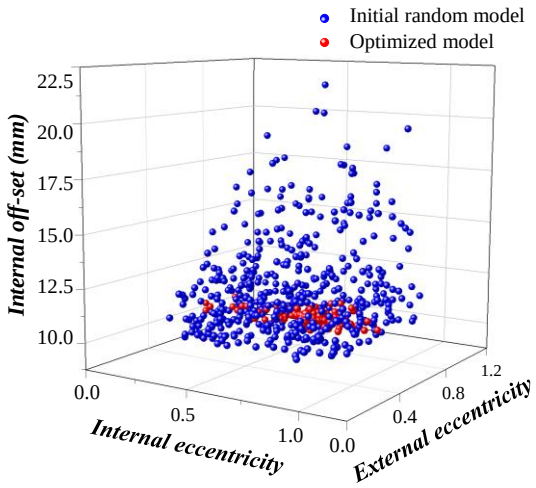

Fig. 4. Particle distribution for initial random model and optimized model.

TABLE I
DIMENSIONS OF THE PROPOSED ILA

Design Parameter	Lower Bounds	Upper Bounds	PSO-Optimum
r_1	25 mm	40 mm	30 mm
r_2	25 mm	50 mm	40 mm
d_{in}	10 mm	25 mm	10 mm
R_1	60 mm	200 mm	120 mm
R_2	60 mm	200 mm	120 mm
d_{ex}	10 mm	25 mm	10 mm

C. PSO-driven Optimization of the Geometry of the Dielectric Lens

For the PSO-driven design exploration of the ray-tracing 2-D model of the dome-shaped dielectric lens, the radii of its internal elliptically curved boundary (r_1 and r_2) with the internal off-set (d_{in}) and the radii of its external elliptically curved boundary (R_1 and R_2) with the external off-set (d_{ex}) are the most critical design parameters. Their search ranges are shown in Table I. Note that the search ranges in Table I have been meticulously decided to ensure that any set of parametric values generated by the PSO algorithm during the global optimization procedure is feasible for the update of the numerical model of the ILA and its subsequent fabrication. For example, considering the machining equipment and manufacturing technology to be used and to ensure geometric congruity, the minimum internal elliptical radii (r_1 and r_2) must be over 25 mm, the external elliptical radii (R_1 and R_2) must be greater than the internal elliptical radii (r_1 and r_2), and the separation between the feeding source (from the phased array) and the dome-shaped lens (h) must be set to 10 mm for the integration with the 8×16 phased array antenna.

The optimization goal is to achieve wide-angle scanning and mitigation of beam scanning loss. With a dielectric constant or relative permittivity (ε_r) of 3.20, the ILA's target scanning angles for normal (0˚) and oblique (15˚, 30˚, 45˚) incidences are deduced to be 0˚, 30˚, 60˚, 78˚, respectively. Due to the inherent limitations of the GO-based estimation, reflection losses at the interface and absorption losses are not considered as part of optimization requirements. Rather, the HPBW is used to formulate the objective function (C_{ILA}) for the suppression of the gain drops due to wider beamwidth in the optimization procedure as follows:

$$C_{\mathrm{ILA}} = \sum_{i=0^\circ,15^\circ,30^\circ,45^\circ}(\mathrm{HPBW_i} - \tau) \times \sigma(\mathrm{HPBW_i}) \quad (6)$$

$$\tau \leq \min(\sum_{i=0^\circ,15^\circ,30^\circ,45^\circ} \mathrm{HPBW_i}) \quad (7)$$

where $\mathrm{HPBW_i}$ is a half-power beamwidth of each output scanning angle, which corresponds to four input angles (0˚, 15˚, 30˚, 45˚). A summation of half-power beamwidth (τ) is required to minimize for reducing the beam widening loss. By minimizing the multiplication of the summation, the PSO-driven global optimization procedure is directed towards achieving a uniform beamwidth distribution among output scanning beams for the proposed ILA.

A swarm size of 500, cognitive and social parameters with values of 3 and 1, respectively, inertia weight boundary of [0.90, 1.20], a minimum neighborhood size of 4, and a total of 10,000 iterations are the algorithmic settings used for the PSO. During the optimization process, the internal and external eccentricities (r_1, r_2, R_1, R_2) and internal off-set (d_{in}) are dominant geometrical parameters as illustrated in Fig. 4.

After 10,000 iterations, PSO converges and the optimal design is shown in Table I.

D. Full-wave Simulation

The PSO-optimized geometry of the dome-shaped dielectric lens is integrated with the 8×16 phased array antenna for the EM model of the proposed ILA in Ansys EDT-HFSS. The proposed ILA is then simulated to verify its wide-angle scanning and scan loss mitigating radiation characteristics when phase delay between adjacent elements is varied from 0˚ to 150˚ with a step size of 15˚. Fig. 5 (a) demonstrates the continuous beam scanning of the estimated normalized gain, where the maximum gain of 20.8 dBi is situated at 0˚. The maximum scan loss at 39.0 GHz is 2.20 dB when the main beam peak is located at 85˚, and the sidelobe level is 10.22 dB when the phase delay difference between adjacent elements is 150˚. Due to the GO assumption, which only considers refractions by Snell's law, wide-angle scanning abilities are applied regardless of frequency. From the simulation results, this broadband operation of wide-angle scanning and scan loss mitigation is validated from 35.0 GHz to 42.0 GHz, as demonstrated in Fig. 5 (b).

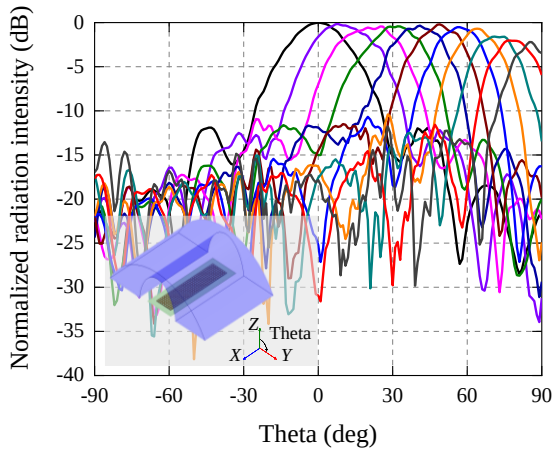

(a)

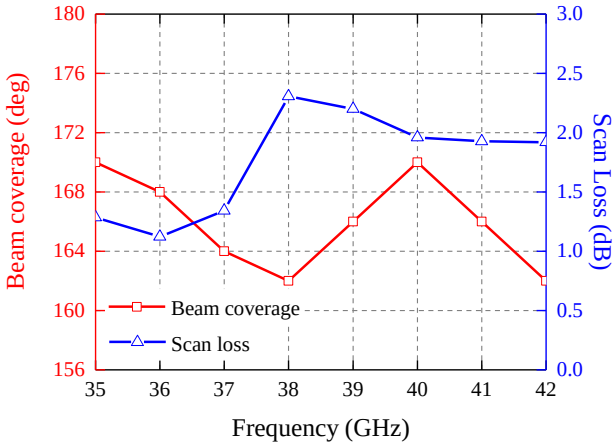

(b)

Fig. 5. (a) Estimated normalized radiation intensity of the devised ILA at 39.0 GHz (b) beam coverage and scan loss from 35.0 GHz to 42.0 GHz.

III. Experimental Validation

The aforementioned approach is experimentally verified through fabrication and measurement of the wide-angle scanning ILA. Due to realistic restrictions in accessing low loss substrates as an academic institution, MC Nylon (ε_r = 3.20, tan (δ) = 0.02) is used to devise the dielectric lens. Nevertheless, in Fig. 6 (a), the fabricated dielectric lens is integrated with the reconfigurable beamforming array for experimental verifications. The radiation patterns are measured by receiving the average power of signals in an anechoic far-field chamber. The received power is converted to the far-field radiation gain of the ILA. Fig. 6 (b) presents the normalized radiation intensities (simulation and measurement), which are normalized values according to their maximum gain at 0˚, respectively. The phase delay range of the beamforming module is varied from 0˚ to 135˚ using a step size of 45˚. When the phase delay is set to 135˚, the main beam peak is located at 78˚ and the measured gain is 17.84 dBi. At this maximum steering angle, the scan loss is 2.10 dB and the sidelobe level is 11.68 dB at 39.0 GHz. The PSO-optimized ILA geometry based on the GO-based multiple scattering (GOMS) is then validated by comparing the

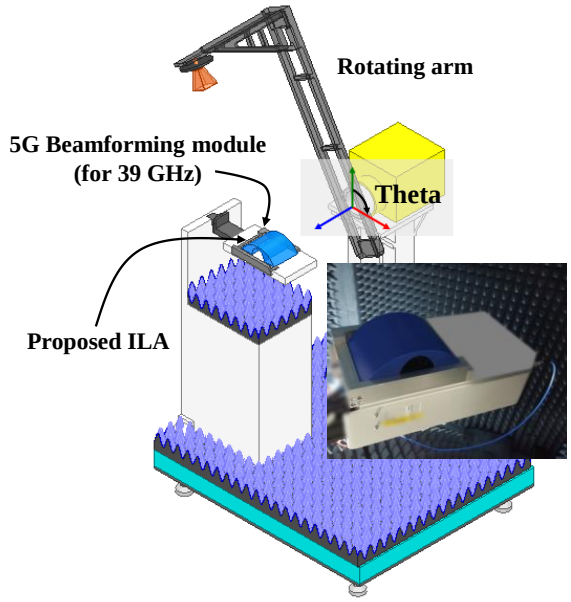

(a)

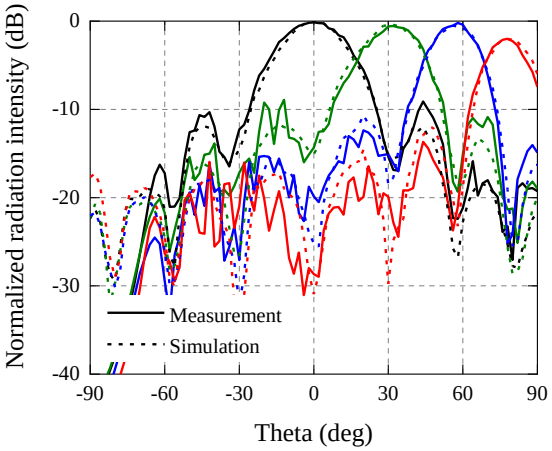

(b)

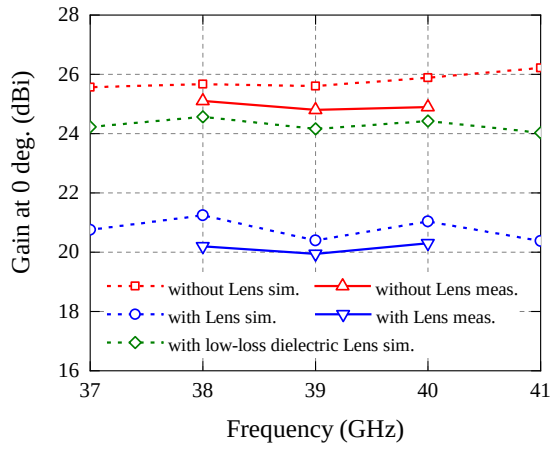

(c)

Fig. 6. (a) Measurement setup (b) measured and simulated radiation pattern at 39.0 GHz (c) measured and simulated gains versus frequencies.

beam's scanning abilities using full-wave simulations and measurements. In addition, the measured and simulated gains versus frequencies are presented in Fig. 6 (c) to specify the loss factors of the ILA. Discrepancies between the simulation and measurement results are 0.8 dB (without lens) and 0.9 dB (with lens), respectively. Furthermore, the loss contribution of the ILA is summarized in Table II. Reduced gain by the lens is analyzed by the difference between the input beam gain (without the lens) and output beam gain (with the lens). From the ratio of the input beam HPBW (without the lens) to output beam HPBW (with the lens), the beam widening loss is calculated. The dielectric material loss is a dominant loss factor, as demonstrated in Table II. In Fig. 6 (c), this high material loss can be mitigated by adopting low-loss dielectrics such as Polyoxymethylene, which has a relative permittivity of 3.20 and loss tangent of 0.002.

TABLE II
LOSS ANALYSIS OF THE ILA PROTOTYPE AT 39.0 GHZ

Output Beam Angle (Input Beam Angle)	Reduced Gain	Beam Widening Loss	Material Loss
0° (0°)	5.0 dB	2.2 dB	2.8 dB
30° (15°)	5.5 dB	1.7 dB	3.8 dB
60° (30°)	4.4 dB	1.2 dB	3.2 dB
78° (45°)	4.6 dB	0.2 dB	4.4 dB

TABLE III
PERFORMANCE COMPARISONS

	[12]	[36]	This work
Design Approach	Optics Only (GO)	Optics Only (GO/PO)	GO-based Multiple Scattering (GOMS)
Topology	GRIN Lens	Polynomial Conics	Off-centered Double-ellipses
Material	3 dielectrics	2 dielectrics	Single dielectric
Scan angle	± 58°*, **	± 70°*, **	± 83°*, ± 78°**
Scan loss	3.0 dB*, 4.1 dB**	1.6 dB*, 3.6 dB**	2.2 dB*, 2.1 dB**
Bandwidth	27.0 ~ 29.0 GHz*	12.0 ~ 14.0 GHz.	35.0 ~ 42.0 GHz*
Fabrication	3D Printing	Machining	Machining

* Simulation, **Measurement

In Table III, the ILA performance is compared to other recent benchmark works. By considering sequential geometric optics and multiple scattering simultaneously, the proposed ILA exhibits a wide-beam scan range of ± 83° (full-wave simulation) and ± 78° (measurement). It features wide-beam coverage, low scan loss and broad operational bandwidth from 35.0 GHz to 42.0 GHz, in comparison to other recent works. In addition, this single dielectric ILA is fabricated by concise machining manufacturing techniques without assembly misalignments.

IV. Conclusion

This paper presents an accurate and efficient ILA design approach for wide-beam coverage of 156° and enhanced scan loss mitigation using a GO-based ray-tracing model estimation and PSO. The investigations provide a practical design guideline for handling the coexistence of optics- and RF-considerations in which high-order, non-linear design parameters have to be analyzed by time-consuming and inefficient conventional computation. For instance, this method can be applied to three-dimensional beamforming applications by adopting the elevation angle when calculating the elevation beamwidth in the ray-tracing model and the objective function. The proposed ILA is expected to contribute to the reduction of infrastructure cost owing to its doubling of the beam coverage, in effect improves the management efficiency of base stations which through a reduction in the total number of hardware required in mmWave wireless networks.

References

[1] Rappaport, Theodore S., et al. "Millimeter wave mobile communications for 5G cellular: It will work!" *IEEE Access*, vol. 1, pp. 335-349, 2013.

[2] Samimi, Mathew K., Theodore S. Rappaport, and George R. MacCartney. "Probabilistic omnidirectional path loss models for millimeter-wave outdoor communications." *IEEE Wireless Communications Letters*, vol. 4, no. 4, pp. 357-360, Aug.2015.

[3] Malila, Bessie, Olabisis Falowo, and Neco Ventura. "Millimeter wave small cell backhaul: An analysis of diffraction loss in NLOS links in urban canyons." *IEEE AFRICON*, Addis Ababa, Ethiopia, 2015.

[4] Zhao, Hang, et al. "28 GHz millimeter wave cellular communication measurements for reflection and penetration loss in and around buildings in New York city." *IEEE International Conference on Communications (ICC)*, Budapest, Hungary, 2013.

[5] Rangan, Sundeep, Theodore S. Rappaport, and Elza Erkip. "Millimeter-wave cellular wireless networks: Potentials and challenges." *Proceedings of the IEEE*, vol. 102, no. 3, pp. 366-385, Mar. 2014.

[6] Ge, Xiaohu, et al. "Energy efficiency challenges of 5G small cell networks." *IEEE Communications Magazine*, vol. 55, no. 5, pp. 184-191, May 2017.

[7] Han, Congzheng, et al. "Green radio: radio techniques to enable energy-efficient wireless networks." *IEEE Communications Magazine*, vol. 49, no. 6, pp. 46-54, Jun. 2011.

[8] Noordin, Nurul H., et al. "Antenna array with wide angle scanning properties." *IEEE European Conference on Antennas and Propagation (EUCAP)*, Prague, Czech Republic, 2012.

[9] Komljenovic, Tin, Niksa Burum, and Zvonimir Sipus. "Analysis of spherical lens antennas-comparison of three analysis methods." *IEEE Conference on Microwave Techniques*, Prague, Czech Republic, 2008.

[10] Artemenko, Alexey, et al. "Experimental characterization of E-band two-dimensional electronically beam-steerable integrated lens antennas." *IEEE Antennas and Wireless Propagation Letters*, vol. 12, pp. 1188-1191.

[11] Kim, Ji Hyung, Yong Bae Park, and Sung-Chan Song. "Electromagnetic analysis of a tangent-ogive dielectric radome with a metallic cap." *IEEE Workshop on Antenna Technology (iWAT)*, Seoul, South Korea, 2015.

[12] Qu, Zhishu, et al. "Wide-Angle Scanning Lens Fed by Small-Scale Antenna Array for 5G in Millimeter-Wave Band." *IEEE Transactions on Antennas and Propagation*, vol. 68, no. 5, pp. 3635-3643, May 2020.

[13] J. Budhu and Y. Rahmat-Samii, "A Novel and Systematic Approach to Inhomogeneous Dielectric Lens Design Based on Curved Ray Geometrical Optics and Particle Swarm Optimization," *IEEE Transactions on Antennas and Propagation*, vol. 67, no. 6, pp. 3657-3669, June 2019.

[14] K. Liu, S. Yang, S. -W. Qu, C. Chen and Y. Chen, "Phased Hemispherical Lens Antenna for 1-D Wide-Angle Beam Scanning," *IEEE Transactions on Antennas and Propagation*, vol. 67, no. 12, pp. 7617-7621, Dec. 2019

[15] Sauleau, Ronan, and Barbara Barès. "A complete procedure for the design and optimization of arbitrarily shaped integrated lens antennas." *IEEE Transactions on Antennas and Propagation*, vol. 54, no. 4, pp. 1122-1133, Apr. 2006.

[16] Youngno Youn and Wonbin Hong. "Achieving Hemispherical Beam Coverage for a 39 GHz Integrated Lens featuring Double-Elliptical Boundaries through sequential GO and multiple Scattering." *2021 IEEE International Symposium on Antennas and Propagation and USNC-URSI Radio Science Meeting*, Singapore, 2021.

[17] Y. Youn et al., "PSO-aided ILA Methodology for Hemispherical Beam Coverage and Scan Loss Mitigation," *2020 International Symposium on Antennas and Propagation*, 2021, pp. 153-154.

[18] Wu, Jingjin, et al. "Energy-efficient base-stations sleep-mode techniques in green cellular networks: A survey." *IEEE Communications Surveys & Tutorials*, vol. 17, Iss. 2, pp. 803-826, 2015.

[19] A. Alieldin et al., "A Triple-Band Dual-Polarized Indoor Base Station Antenna for 2G, 3G, 4G and Sub-6 GHz 5G Applications," *IEEE Access*, vol. 6, pp. 49209-49216, 2018.

[20] B. Liu et al., "An Efficient Method for Complex Antenna Design Based on a Self Adaptive Surrogate Model-Assisted Optimization Technique," *IEEE Transactions on Antennas and Propagation*, vol. 69, no. 4, pp. 2302-2315, April 2021.

[21] V. Grout, M. O. Akinsolu, B. Liu, P. I. Lazaridis, K. K. Mistry and Z. D. Zaharis, "Software Solutions for Antenna Design Exploration: A Comparison of Packages, Tools, Techniques, and Algorithms for Various Design Challenges," *IEEE Antennas and Propagation Magazine*, vol. 61, no. 3, pp. 48-59, June 2019.

[22] Werner D., Gregory M., Jiang Z.H., Brocker D.E. (2015) Optimization Methods in Antenna Engineering. In: Chen Z. (eds) *Handbook of Antenna Technologies*. Springer, Singapore.

[23] S. Koziel and S. Ogurtsov. Antenna design by simulation-driven optimization. Cham, Switzerland: Springer International Publishing, 2014.

[24] J. Zhang et al., "Automatic AI-Driven Design of Mutual Coupling Reducing Topologies for Frequency Reconfigurable Antenna Arrays," *IEEE Transactions on Antennas and Propagation*, vol. 69, no. 3, pp. 1831-1836, March 2021.

[25] M. Alibakhshikenari et al., "Dual-Polarized Highly Folded Bowtie Antenna with Slotted Self-Grounded Structure for Sub-6 GHz 5G Applications," *IEEE Transactions on Antennas and Propagation*, 2021.

[26] M. Kovaleva, D. Bulger and K. P. Esselle, "Comparative Study of Optimization Algorithms on the Design of Broadband Antennas," *IEEE Journal on Multiscale and Multiphysics Computational Techniques*, vol. 5, pp. 89-98, 2020.

[27] X. Li and K. M. Luk, "The Grey Wolf Optimizer and Its Applications in Electromagnetics," *IEEE Transactions on Antennas and Propagation*, vol. 68, no. 3, pp. 2186-2197, March 2020.

[28] E. N. Tziris, P. I. Lazaridis, Z. D. Zaharis, J. P. Cosmas, K. K. Mistry and I. A. Glover, "Optimized Planar Elliptical Dipole Antenna for UWB EMC Applications," *IEEE Transactions on Electromagnetic Compatibility*, vol. 61, no. 4, pp. 1377-1384, Aug. 2019

[29] A. A. Al-Azza, A. A. Al-Jodah and F. J. Harackiewicz, "Spider Monkey Optimization: A Novel Technique for Antenna Optimization," *IEEE Antennas and Wireless Propagation Letters*, vol. 15, pp. 1016-1019, 2016.

[30] P. I. Lazaridis et al., "Comparison of evolutionary algorithms for LPDA antenna optimization," *Radio Science*, vol. 51, no. 8, pp. 1377-1384, Aug. 2016.

[31] Q. Wu, Y. Cao, H. Wang and W. Hong, "Machine-learning-assisted optimization and its application to antenna designs: Opportunities and challenges," *China Communications*, vol. 17, no. 4, pp. 152-164, April 2020

[32] Z. Zhang, H. C. Chen and Q. S. Cheng, "Surrogate-Assisted Quasi-Newton Enhanced Global Optimization of Antennas Based on a Heuristic Hypersphere Sampling," *IEEE Transactions on Antennas and Propagation*, vol. 69, no. 5, pp. 2993-2998, May 2021.

[33] Q. Hua et al., "A Novel Compact Quadruple-Band Indoor Base Station Antenna for 2G/3G/4G/5G Systems," *IEEE Access*, vol. 7, pp. 151350-151358, 2019.

[34] Tang, Zhaoyang, et al. "A wideband differentially fed dual-polarized stacked patch antenna with tuned slot excitations." *IEEE Transactions on Antennas and Propagation*, vol. 66, no. 4, pp. 2055-2060, Apr. 2018.

[35] Fernandes, Carlos A., Eduardo B. Lima, and Jorge R. Costa. "Dielectric lens antennas." *Handbook of antenna technologies*, pp. 1001-1064.

[36] Gandini, Erio, et al. "A Dielectric Dome Antenna with Reduced Profile and Wide Scanning Capability." *IEEE Transactions on Antennas and Propagation*, vol. 69, no. 2, pp. 747-759, Feb. 2021.